Progress In Electromagnetics Research M, Vol. 47, 67–76, 2016

Study of the Shielding Effectiveness of Double Rectangular Enclosures with Apertures Excited by an Internal Source

Jian-Hong Hao, Lu-Hang Jiang*, Yan-Fei Gong, and Jie-Qing Fan

Abstract—An analytical formulation has been developed to evaluate the shielding effectiveness (SE) of two coplanar rectangular metallic enclosures with a circular aperture excited by an internal electric dipole source. The formulation consists of three parts: First, the near-field electromagnetic interference (EMI) of the electromagnetic leakage from the aperture is represented by the electric dipole in one enclosure. Then, the aperture equivalent magnetic and electric dipole moments are calculated according to the Bethe's small aperture coupling theory. Finally, the electric field of the other enclosure is derived by using the equivalent magnetic dipole field, equivalent electric dipole field and the corresponding enclosure's Green's functions in the two fields. In this formulation, the electric field of the enclosure can be expressed as a function of the observation point, the aperture's center point, source point, shape of the aperture and enclosure's conductivity. The formulation then is employed to analyze the effect of the above factors on the SE. The analytical results have been successfully compared with the full-wave simulation software Computer Simulation Technology (CST) from $0.3 \sim 2.4$ GHz.

1. INTRODUCTION

Electromagnetic field coupling into a metallic enclosure through apertures has become an important issue in recent years. The shielding effectiveness (SE) of a mono-enclosure [1–3] or multiple enclosures [4–6] with apertures has been especially studied by using numerical methods and analytical formulations. Numerical methods, including the finite difference time domain (FDTD) method [7, 8], finite element method (FEM) [9], method of moments (MoM) [10, 11], and transmission-line modeling (TLM) method [12], are robust and accurate but always require large computational resources. Analytical formulations such as the Bethe's small aperture coupling theory [13–15], equivalent circuit method [1–3, 16] and BLT equation [6, 17], although approximate, are much faster than numerical methods, and more convenient in investigating the effect of design parameters on the SE. The SE of a shielding enclosure is defined as the ratio of field strengths in the presence and absence of the enclosure.

The SE of double rectangular enclosures with apertures against an external plane wave is investigated in [4–6]. It is far-field electromagnetic interference (EMI), and the field source is placed outside the enclosure. However, there exist lots of situations in which the field source is required to be placed inside the enclosure. The electromagnetic leakage of an apertured rectangular enclosure excited by an internal electric dipole is studied in [15]. The electromagnetic field coupling with a transmission line located in a rectangular enclosure excited by an internal electric dipole is studied in [18]. In fact, with the rapid development of large-scale integrated circuit, the enclosure is always divided into several regions mainly to reduce the near-field EMI from electronic devices and components of adjacent enclosures through the apertures. Unlike far-field EMI, near-field EMI is more complex and destructive. Therefore, it is necessary to study the universal near-field EMI between adjacent enclosures.

In this paper, an analytical formulation has been developed to evaluate the SE of two coplanar rectangular metallic enclosures with a circular aperture excited by an internal electric dipole. First,

Received 25 January 2016, Accepted 21 March 2016, Scheduled 27 March 2016
* Corresponding author: Lu-Hang Jiang (13261200137@163.com).
The authors are with the Department of Electrical and Electronic Engineering, North China Electric Power University, Beijing, China.

the near-field EMI of the electromagnetic leakage from the aperture is represented by the electric dipole in one enclosure. Then, the aperture equivalent magnetic and electric dipole moments are calculated according to the Bethe's small aperture coupling theory. Finally, the electric field of the other enclosure is derived by using the equivalent magnetic dipole field, equivalent electric dipole field and the corresponding enclosure's Green's functions in the two fields. In [4], the rectangular aperture coupling with large length-width ratio is studied, and the aperture's radiation can be represented only with the magnetic polarizability, considering the negligible contribution of the electric polarizability. In our model, both of the magnetic and electric polarizabilities are taken into consideration in order to study the circular aperture coupling. Therefore, the analytical formulation proposed is more accurate in most of the frequency band from $0.3 \sim 2.4$ GHz than the model in which only the magnetic polarizability is considered in evaluating the SE of the enclosure.

The rest of the paper is organized as follows. Section 2 presents the geometry and mathematical formulas of the analytical model. Section 3 illustrates the verification with a conventional full-wave simulation tool CST and analyzes the effect of some parameters of the enclosure on the SE. Finally, some conclusions are drawn in Section 4.

2. THEORY

2.1. Analytical Model

The geometry of the analytical model is shown in Figure 1. It consists of two coplanar rectangular metallic enclosures (enclosure 1 and enclosure 2) with a circular aperture on the plane $z = z_e$ excited by an electric dipole in enclosure 1. The dimensions of the enclosures are both $x_e \times y_e \times z_e$. The diameter of the aperture is d, and the center point of the aperture is located at $P_0(x_0, y_0, z_0)$. The source interference is an electric dipole oriented along the y-axis located at $P_s(x_s, y_s, z_s)$. The SE observation point is located at $P(x, y, z)$ in enclosure 2.

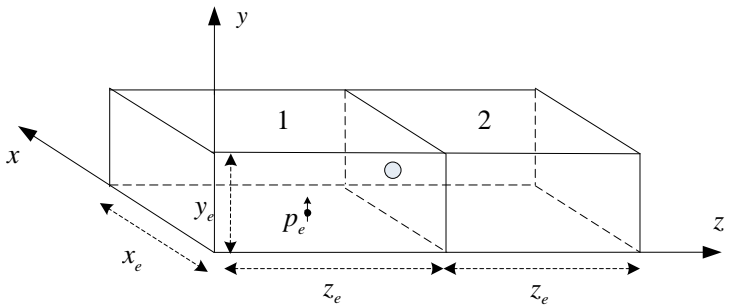

Figure 1. Double rectangular metallic enclosures with a circular aperture excited by an internal electric dipole.

According to the Bethe's small aperture coupling theory, usually when the diameter of the circular aperture is shorter than 1/10 wavelength of interest, the leakage field of enclosure 2 can be represented by the aperture equivalent electric and magnetic dipole moments $\mathbf{p}$ and $\mathbf{m}$ [13]. The equations linking the dipole moments and the unperturbed fields of enclosure 1, when it is totally closed, are [15]

$$\mathbf{p} = \alpha_{ez}\varepsilon_0 E_{u,z}\mathbf{e}_z \tag{1}$$

$$\mathbf{m} = -\alpha_{mx}H_{u,x}\mathbf{e}_x - \alpha_{my}H_{u,y}\mathbf{e}_y \tag{2}$$

where ε_0 is the electric permittivity of vacuum; $E_{u,z}$ is the unperturbed electric field along the z-axis; $H_{u,x}$ and $H_{u,y}$ are the unperturbed magnetic field along the x-axis and y-axis, respectively; α_{ez}, α_{mx} and α_{my} are the electric polarizability along the z-axis, magnetic polarizability along the x-axis and magnetic polarizability along the y-axis, respectively. The polarizability is dependent only upon the shape and size of the aperture.

For a circular aperture with diameter d, the polarizability is [19]

$$\alpha_{ez} \approx d^3/6, \quad \alpha_{mx} = \alpha_{my} = d^3/3 \tag{3}$$

$E_{u,z}$, $H_{u,x}$ and $H_{u,y}$ are given by [15]

$$E_{u,z} = \frac{-j\omega\mu_0 Idl}{k^2(x_e y_e z_e)} \sum_{n=0}^{\infty}\sum_{l=0}^{\infty} \Gamma_{nl}\left(\frac{y_e}{2}\right) \times \{\sin k_1[y_e - (y_0 + y_s)] + \mathrm{sgn}(y_0 - y_s)\sin k_1(y_e - |y_0 - y_s|)\} \times \sin(k_1 y_e)^{-1} \quad (4)$$

$$H_{u,x} = \frac{-Idl}{(x_e y_e z_e)} \sum_{n=0}^{\infty}\sum_{l=0}^{\infty} \Gamma_{nl}\left(\frac{y_e}{2k_1}\right) \times [\cos k_1(y_0 + y_s - y_e) + \cos k_1(|y_0 - y_s| - y_e)] \times \sin(k_1 y_e)^{-1} \quad (5)$$

$$H_{u,y} = 0 \quad (6)$$

where $\omega = 2\pi f$; μ_0 is the magnetic permeability of vacuum; k is the free space wavenumber; I and dl are the current and length of the electric dipole, respectively; n and l are the field mode number along the x-axis and z-axis, respectively.

$$k_1 = \sqrt{k^2 - (n\pi/x_e)^2 - (l\pi/z_e)^2} \quad (7)$$

$$\Gamma_{nl} = \varepsilon_{0n}\varepsilon_{0l}\left(\frac{l\pi}{z_e}\right)\cos\left(\frac{l\pi z_0}{z_e}\right)\sin\left(\frac{l\pi z_s}{z_e}\right)\sin\left(\frac{n\pi x_0}{x_e}\right)\sin\left(\frac{n\pi x_s}{x_e}\right) \quad (8)$$

where ε_{0n} and ε_{0l} are Neumann factors, $\varepsilon_{0n(l)} = 1$ for $n(l) = 0$ and $\varepsilon_{0n(l)} = 2$ for $n(l) \neq 0$.

2.2. Electric Field and SE Calculation for the Magnetic Polarizability

When the equivalent magnetic dipole moment is considered, enclosure 2's Green's function is presented as follows [14]:

$$G_m = -\sum_{n=0}^{\infty}\sum_{m=0}^{\infty}\left(\frac{\varepsilon_{0n}\varepsilon_{0m}}{x_e y_e}\right)\left[\frac{\sin(k_x x_0)\cos(k_y y_0)}{k_{nm}\sin(k_{nm} z_e)}\right]\sin(k_x x)\cos(k_y y) \times \{\cos[k_{nm}(|z + z_0| - z_e)] + \cos[k_{nm}(|z - z_0| - z_e)]\} \quad (9)$$

where ε_{0m} is Neumann factor, $\varepsilon_{0m} = 1$ for $m = 0$ and $\varepsilon_{0m} = 2$ for $m \neq 0$. $k_x = n\pi/x_e$, $k_y = m\pi/y_e$, $k_{nm} = \sqrt{k^2 - k_x^2 - k_y^2}$. m is the field mode number along the y-axis.

The electric field $\mathbf{E}$ is related to $\mathbf{G}_m$ as follows:

$$\mathbf{E} = -j\omega\mu_0\alpha_{mx}H_{u,x}(\nabla \times \mathbf{G}_m) \quad (10)$$

Substituting Eq. (9) into Eq. (10), the electric field components of enclosure 2 may be derived as follows:

$$E_{mx} = 0 \quad (11)$$

$$E_{my} = -j\omega\mu_0\alpha_{mx}H_{u,x}\sum_{n=0}^{\infty}\sum_{m=0}^{\infty}\left(\frac{\varepsilon_{0n}\varepsilon_{0m}}{x_e y_e}\right)\left[\frac{\sin(k_x x_0)\cos(k_y y_0)}{\sin(k_{nm} z_e)}\right]\sin(k_x x)\cos(k_y y) \times \{\sin[k_{nm}(z_e - |z + z_0|)] + \mathrm{sgn}(z - z_0)\sin[k_{nm}(z_e - |z - z_0|)]\} \quad (12)$$

$$E_{mz} = -j\omega\mu_0\alpha_{mx}H_{u,x}\sum_{n=0}^{\infty}\sum_{m=0}^{\infty}\left(\frac{\varepsilon_{0n}\varepsilon_{0m}}{x_e y_e}\right)k_y\left[\frac{\sin(k_x x_0)\cos(k_y y_0)}{k_{nm}\sin(k_{nm} z_e)}\right]\sin(k_x x)\sin(k_y y) \times \{\cos[k_{nm}(|z + z_0| - z_e)] + \cos[k_{nm}(|z - z_0| - z_e)]\} \quad (13)$$

We can therefore calculate the SE for the magnetic polarizability at observation point P by superposition of the electric field components.

$$E_m = \sqrt{E_{mx}^2 + E_{my}^2 + E_{mz}^2} \quad (14)$$

$$SE_m = -20\log_{10}\left(\frac{|E_m|}{|E_0|}\right) \quad (15)$$

where E_0 is the electric field at P in the absence of both enclosure 1 and enclosure 2.

2.3. Electric Field and SE Calculation for the Electric Polarizability

Similarly, when the equivalent electric dipole moment is considered, enclosure 2's Green's function is presented as follows:

$$G_e = \sum_{n=0}^{\infty}\sum_{m=0}^{\infty}\sum_{l=0}^{\infty}\left(\frac{c^2}{x_e y_e z_e}\right)\left[\frac{\cos(k_x x_0)\cos(k_y y_0)\sin(k_z z_0)}{\omega_{nml}^2-\omega^2}\right]\cos(k_x x)\cos(k_y y)\sin(k_z z) \tag{16}$$

where c is the velocity of light of vacuum, $k_z = l\pi/z_e$, $\omega_{nml} = \sqrt{k_x^2+k_y^2+k_z^2-k^2}\Big/c^2$.

Equation (16) is a triple series. In order to improve its convergence rate, it is simplified as Equation (18) by using identical Equation (17)

$$\sum_{n=1}^{\infty}\frac{\cos nx}{n^2-a^2} = \frac{1}{2a^2}-\frac{\pi}{2a^2}\frac{\cos(x-n)a}{\sin\pi a}(0\le x\le 2\pi) \tag{17}$$

$$\begin{aligned} G_e &= \sum_{n=0}^{\infty}\sum_{m=0}^{\infty}\left(\frac{\varepsilon_{0n}\varepsilon_{0m}}{x_e y_e}\right)\left[\frac{\cos(k_x x_0)\cos(k_y y_0)}{k_{nm}\sin(k_{nm} z_e)}\right]\cos(k_x x)\cos(k_y y) \\ &\quad\times\{\cos[k_{nm}(|z+z_0|-z_e)]-\cos[k_{nm}(|z-z_0|-z_e)]\} \end{aligned} \tag{18}$$

The electric field $\mathbf{E}$ is related to $\mathbf{G}_e$ as follows:

$$\mathbf{E} = -(j\omega\alpha_e\varepsilon_0 E_{u,z})\times\left[(1/j\omega\mu_0\varepsilon_0)\nabla\left(\varepsilon_0\frac{\partial G_e}{\partial z}\right)-j\omega\varepsilon_0 G_e\mathbf{e}_z\right] \tag{19}$$

Substituting Eq. (18) into Eq. (19), the electric field components of enclosure 2 may be derived as follows:

$$\begin{aligned} E_{ex} &= -(j\omega\alpha_e\varepsilon_0 E_{u,z})\frac{1}{j\omega\mu_0}\sum_{n=0}^{\infty}\sum_{m=0}^{\infty}\left(\frac{\varepsilon_{0n}\varepsilon_{0m}}{x_e y_e}\right)k_x\left[\frac{\cos(k_x x_0)\cos(k_y y_0)}{\sin(k_{nm} z_e)}\right]\sin(k_x x)\cos(k_y y) \\ &\quad\times\{\sin[k_{nm}(z_e-|z+z_0|)]-\mathrm{sgn}(z-z_0)\sin[k_{nm}(z_e-|z-z_0|)]\} \end{aligned} \tag{20}$$

$$\begin{aligned} E_{ey} &= -(j\omega\alpha_e\varepsilon_0 E_{u,z})\frac{1}{j\omega\mu_0}\sum_{n=0}^{\infty}\sum_{m=0}^{\infty}\left(\frac{\varepsilon_{0n}\varepsilon_{0m}}{x_e y_e}\right)k_y\left[\frac{\cos(k_x x_0)\cos(k_y y_0)}{\sin(k_{nm} z_e)}\right]\cos(k_x x)\sin(k_y y) \\ &\quad\times\{\sin[k_{nm}(z_e-|z+z_0|)]-\mathrm{sgn}(z-z_0)\sin[k_{nm}(z_e-|z-z_0|)]\} \end{aligned} \tag{21}$$

$$\begin{aligned} E_{ez} &= -(j\omega\alpha_e\varepsilon_0 E_{u,z})\frac{1}{j\omega\mu_0}\sum_{n=0}^{\infty}\sum_{m=0}^{\infty}\left(\frac{\varepsilon_{0n}\varepsilon_{0m}}{x_e y_e}\right)k_{nm}\left[\frac{\cos(k_x x_0)\cos(k_y y_0)}{\sin(k_{nm} z_e)}\right]\cos(k_x x)\cos(k_y y) \\ &\quad\times\{\cos[k_{nm}(z+z_0-z_e)]+\cos[k_{nm}(|z-z_0|-z_e)]\} \end{aligned} \tag{22}$$

We can therefore calculate the SE for the electric polarizability at observation point P by superposition of the electric field components.

$$E_e = \sqrt{E_{ex}^2+E_{ey}^2+E_{ez}^2} \tag{23}$$

$$SE_e = -20\log_{10}\left(\frac{|E_e|}{|E_0|}\right) \tag{24}$$

2.4. Electric Field and SE Calculation for Both of the Magnetic and Electric Polarizabilities

We can therefore calculate the total electric field components by superposition of E_m components and E_e components

$$E_x = E_{mx}+E_{ex},\quad E_y = E_{my}+E_{ey},\quad E_z = E_{mz}+E_{ez} \tag{25}$$

Finally, we can calculate the total SE at the observation point by superposition of the total electric field components

$$E = \sqrt{E_x^2 + E_y^2 + E_z^2} \tag{26}$$

$$SE = -20\log_{10}\left(\frac{|E|}{|E_0|}\right) \tag{27}$$

3. RESULTS AND DISCUSSIONS

In this section, the SE of the observation point is calculated by using the analytical model proposed in Section 2. Various configurations including different positions of the observation point, aperture's center point and electric dipole, different shapes of the aperture, and different conductivities of the enclosure are studied. So for verifying it, our results are compared with the CST simulation results in the frequency range $0.3 \sim 2.4$ GHz. It is important to notice that the electric dipole is oriented along the y-axis in our model, so only the electric field along the y-axis and the magnetic field along the x-axis have been considered in calculating the SE.

In Section 3.1, the SE for the magnetic polarizability, the SE for the electric polarizability, and the total SE for both of the magnetic and electric polarizabilities are calculated, respectively. The dimensions of the double enclosures are both 300 mm×120 mm×300 mm. The aperture radius is $r = 5$ mm. The aperture's center point is located at P_0 (150, 60, 300) mm. The electric dipole and observation point are located at P_s (150, 60, 20) mm and P (150, 60, 450) mm, respectively. In Section 3.2, the effect of various parameters of the enclosure on the SE is analyzed.

3.1. Model Validation

Figure 2, Figure 3 and Figure 4 show the calculated SE for the magnetic polarizability, the SE for the electric polarizability and the total SE for both of the magnetic and electric polarizabilities respectively using the analytical model and the results from the CST. It can be seen that three resonant modes, TE_{101}, TE_{301} and TE_{303}, have been identified corresponding to the enclosure resonant frequencies, 0.71 GHz, 1.58 GHz and 2.12 GHz, respectively. Figure 5 shows the comparison of the calculated SE for the magnetic polarizability, electric polarizability and both of the magnetic and electric polarizabilities. In comparison of Figures 2, 3, 4 and 5, it can be seen that the result of Figure 4 is more accurate than that of Figure 2 and Figure 3 from $0.3 \sim 2.12$ GHz, and the result of Figure 2 is more accurate than that

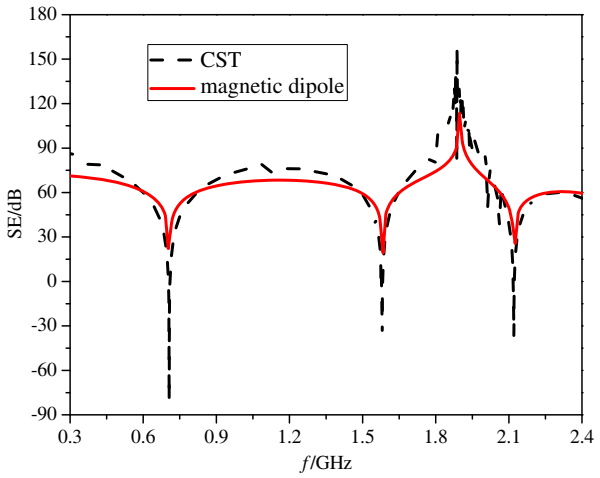

Figure 2. Calculated SE for the magnetic polarizability using the analytical model and the result from CST.

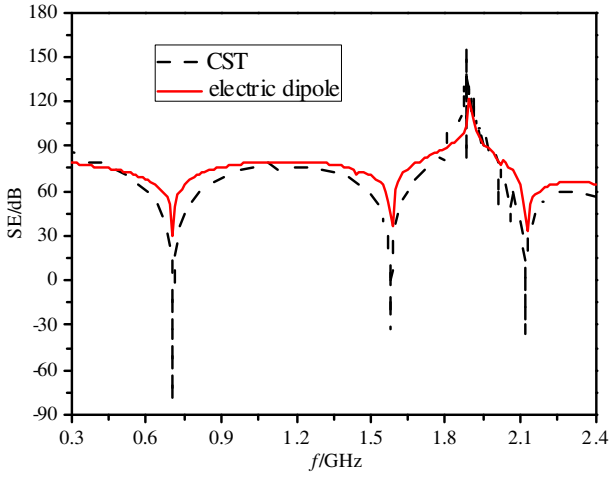

Figure 3. Calculated SE for the electric polarizability using the analytical model and the result from CST.

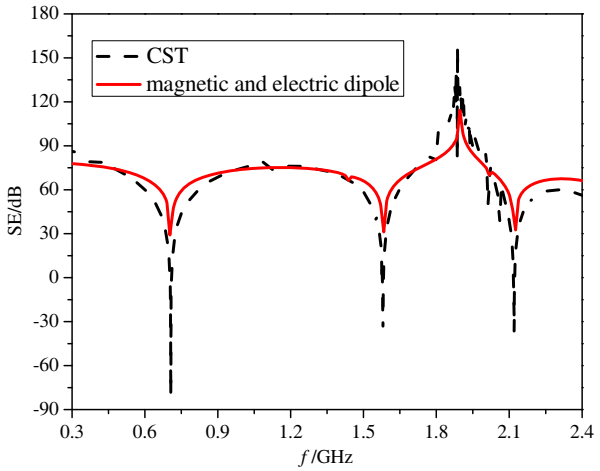

Figure 4. Calculated total SE for both of the magnetic and electric polarizabilities using the analytical model and the result from CST.

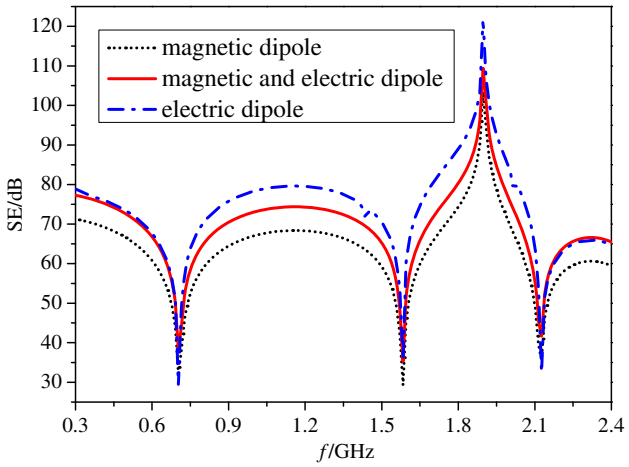

Figure 5. Calculated SE for the magnetic polarizability, the electric polarizability and both of the magnetic and electric polarizabilities.

of Figure 3 and Figure 4 from 2.12 $\sim$ 2.4 GHz. Therefore, it is better to consider both of the magnetic and electric polarizabilities under 2.12 GHz.

3.2. The Effect of Various Parameters on the SE

By keeping the position of the electric dipole and the aperture's center point unvaried, Figure 6 shows the calculated SE for different observation points of (150, 60, 450) mm, (202, 60, 450) mm and (228, 60, 450) mm. It can be seen that the nearer the observation point is to the side wall, the higher the SE will be. It is because when y and z of the observation point are unvaried, while x changes, the electric field depends on the function $|\sin(n\pi x/x_e)|$. If mode n is odd, $|\sin(n\pi x/x_e)|$ decreases monotonically with the increase of independent variable x on the interval [150, 300] mm. The variation of the SE is similar for x on the interval [0, 150] mm, considering the symmetry of the double enclosures about the electric dipole and the aperture. Therefore, the nearer the observation point is to the side wall, the lower the

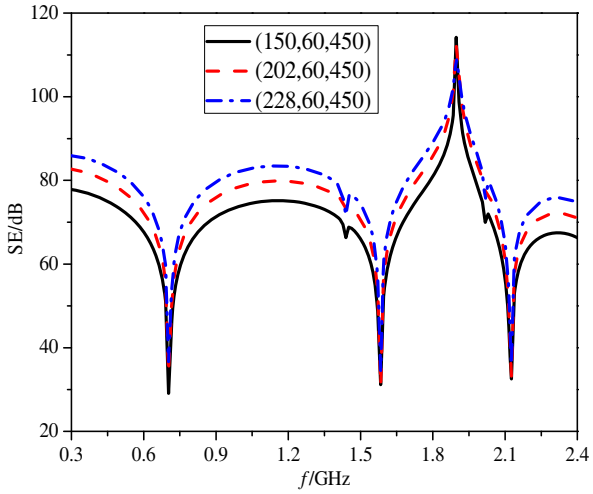

Figure 6. Calculated SE for different observation points with $P_0(x_0, y_0, z_0) = (150, 60, 300)$ mm and $P_s(x_s, y_s, z_s) = (150, 60, 20)$ mm.

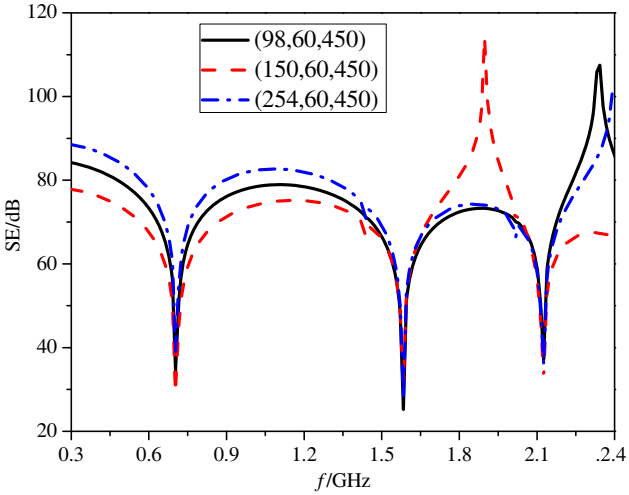

Figure 7. Calculated SE for different aperture's center points with $P_s(x_s, y_s, z_s) = (150, 60, 20)$ mm.

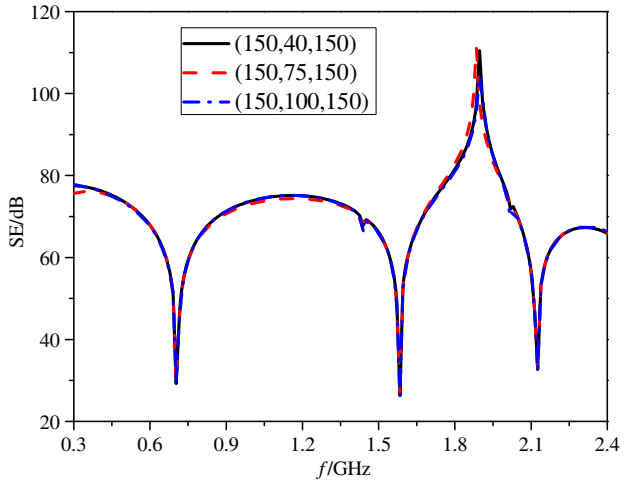

Figure 8. Calculated SE for different positions of the electric dipole with $P_0(x_0, y_0, z_0) = (150,\ 60,\ 300)$ mm and $P(x, y, z) = (150,\ 60,\ 450)$ mm.

electric field will be, and the higher the SE will be.

By keeping the position of the electric dipole unvaried, Figure 7 shows the calculated SE for different aperture's center points of (150, 60, 300) mm, (98, 60, 300) mm and (254, 60, 300) mm. In order to keep the observation points on the central axis of the aperture, they are set at (150, 60, 450) mm, (98, 60, 450) mm and (254, 60, 450) mm, respectively. It can be seen that before the second resonant point, the nearer the aperture's center point is to the side wall, the higher the SE will be. However, that law is not obvious after the second resonant point. In addition, the frequency points where the SE increases rapidly differ in the three graphs. The reason is that the aperture is at zero points of the electric field of the enclosure, which will change for different aperture's center points.

By keeping the aperture's center point at P_0 (150, 60, 300) mm and the observation point at P (150, 60, 450) mm, Figure 8 shows the calculated SE for different electric dipole positions of (150, 40, 150) mm, (150, 75, 150) mm and (150, 100, 150) mm. It can be seen that the SE remains almost the same except in the frequency range at the very beginning. It is because according to Equations (4) and (5), the change of the independent variable y_s of the electric dipole contributes little to the unperturbed electric field component $E_{u,z}$ and the unperturbed magnetic field component $H_{u,x}$. Therefore, the graphs almost keep the same in general.

By changing the polarizability of the aperture, Figure 9 shows the calculated SE for the rectangular aperture using the analytical model and the result from CST. It can be seen that the result from the analytical model is in good agreement with that from CST in most of the frequency band from $0.3 \sim 2.4$ GHz. Figure 10 shows the comparison of the calculated SE for the rectangular aperture and the circular aperture with the same size. It can be seen that the SE of the circular aperture increases about 15 dB compared with that of the rectangular aperture.

The material of the enclosure is perfect conductor in the above model. Next, the effect of the lossy material on the SE of the enclosure will be investigated. It is assumed that only the incident TE_{nm} wave will be considered in the following research. For a rectangular enclosure, the propagation constants γ_1 and γ_{nm} are presented as follows [3]:

$$\gamma_1 = \sqrt{-\beta_0^2 - (1-j)\delta\left[\frac{\varepsilon_{0n}}{x_e}\left(k_{c0}^2 + \beta_0^2\frac{k_x^2}{k_{c0}^2}\right) + \frac{\varepsilon_{0m}}{y_e}\left(k_{c0}^2 + \beta_0^2\frac{k_y^2}{k_{c0}^2}\right)\right]} \tag{28}$$

$$\gamma_{nm} = \sqrt{-\beta_0^2 - (1-j)\delta\left[\frac{\varepsilon_{0n}}{x_e}\left(k_{c0}^2 + \beta_0^2\frac{k_x^2}{k_{c0}^2}\right) + \frac{\varepsilon_{0l}}{z_e}\left(k_{c0}^2 + \beta_0^2\frac{k_z^2}{k_{c0}^2}\right)\right]} \tag{29}$$

where $k_{c0} = \sqrt{k_x^2 + k_y^2}$ is the cutoff wavenumber of the TE_{nm} mode; $\beta_0 = \sqrt{k^2 - k_{c0}^2}$, $\delta = \sqrt{2/(\omega\sigma\mu)}$ is the skin depth of the lossy material; σ and μ are the conductivity and magnetic permeability of the lossy

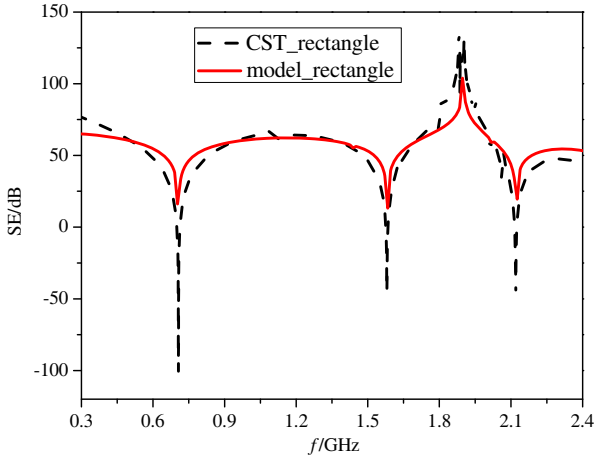

Figure 9. Calculated SE for the rectangular aperture using the analytical model and the result from CST.

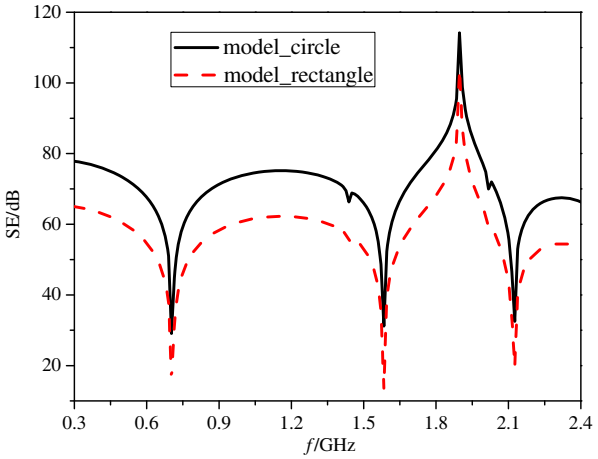

Figure 10. Calculated SE for circular aperture and rectangular aperture with the same size.

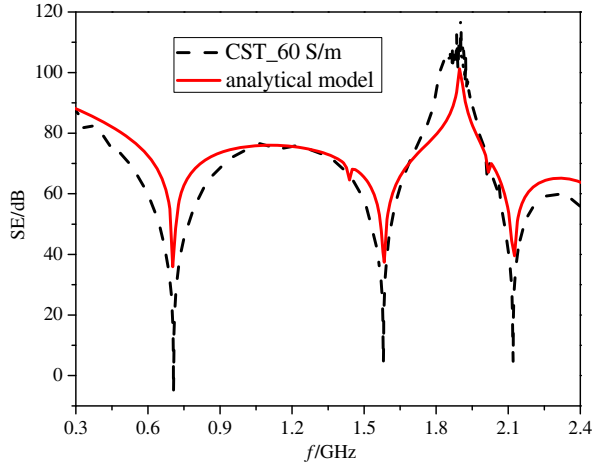

Figure 11. Calculated SE when the enclosure 1 is perfect and the enclosure 2 is lossy with the conductivity of 60 S/m using the analytical model and the result from CST.

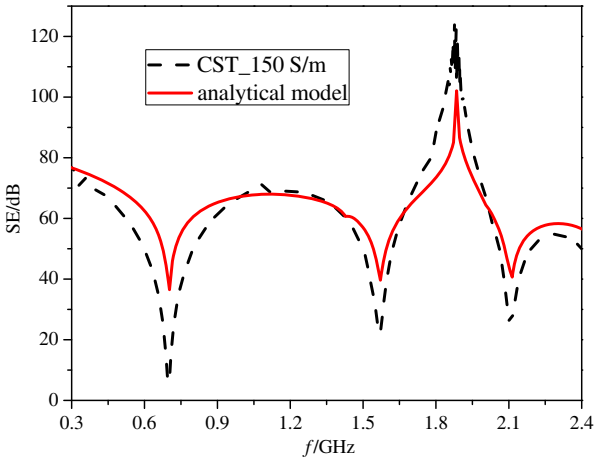

Figure 12. Calculated SE when the enclosure 1 and enclosure 2 are both lossy with the conductivity of 150 S/m using the analytical model and the result from CST.

material, respectively. The electric field of the lossy enclosure can then be derived by the substitution of the parameters k_1 and k_{nm} for the perfect enclosure [3].

$$k_1 = -j\gamma_1, \quad k_{nm} = -j\gamma_{nm} \tag{30}$$

Figure 11 shows the calculated SE for the double enclosures of which enclosure 1 is perfect and enclosure 2 lossy with the conductivity of 60 S/m. Figure 12 shows the calculated SE for the double enclosures which are totally lossy with the conductivity of 150 S/m. It can be seen that the results from the analytical model are in good agreement with those from CST in most of the frequency band from $0.3 \sim 2.4$ GHz. Although the SEs of the lossy enclosure in general have a slight decrease in comparison with those of the perfect enclosure, the lossy material can lead to great suppression of SE reduction resulting from the enclosure resonance effect and significant improvement of the SEs around the resonant frequencies.

4. CONCLUSION

An analytical formulation has been developed to evaluate the SE of two coplanar rectangular metallic enclosures with a circular aperture excited by an internal electric dipole source. The electric field components of the observation points are derived according to the Bethe's small aperture coupling theory and the enclosure's Green's function. The results from the analytical model are in good agreement with those from the full-wave simulation software CST in most of the frequency band from $0.3 \sim 2.4$ GHz. The results show that the observation point, aperture's center point, shape of the aperture, and enclosure's conductivity can all have a significant influence on the SE except the electric dipole source point. It is relatively fast, accurate and convenient to evaluate the SE and analyze the effect of different factors on it by using the analytical formulation proposed in comparison with numerical methods. The results are helpful for guiding the design of more complex electromagnetic shielding enclosures.

ACKNOWLEDGMENT

The authors thank for the funding support from the National Natural Science Foundation (No. 61372050).

REFERENCES

1. Shim, J., D. G. Kam, J. H. Kwon, and J. Kim, "Circuital modeling and measurement of shielding effectiveness against oblique incident plane wave on apertures in multiple sides of rectangular enclosure," *IEEE Trans. Electromagn. Compat.*, Vol. 52, No. 3, 566–577, 2010.
2. Hao, J.-H., P.-H. Qi, J.-Q. Fan, and Y.-Q. Guo, "Analysis of shielding effectiveness of enclosures with apertures and inner windows with TLM," *Progress In Electromagnetic Research M*, Vol. 32, 73–82, 2013.
3. Jiao, C.-Q. and H.-Z. Zhu, "Resonance suppression and electromagnetic shielding effectiveness improvement of an apertured rectangular cavity by using wall losses," *Chin. Phys .B*, Vol. 22, No. 8, 1–6, 2013.
4. Song, H., D.-F. Zhou, D.-T. Hou, T. Hu, and J.-Y. Lin, "Hybrid algorithm for slot coupling of double layer shielding cavity," *High Power Laser and Particle Beams*, Vol. 20, No. 11, 1892–1898, 2008.
5. Hao, C. and D.-H. Li, "Shielding effectiveness of double-deck cavity with apertures," *Chinese Journal of Radio Science*, Vol. 29, No. 1, 114–121, 2014.
6. Luo, J.-W., P.-A. Du, D. Ren, and P. Xiao, "BLT equation-based approach for calculating shielding effectiveness of double layer rectangular enclosures with apertures," *High Power Laser and Particle Beams*, Vol. 27, No. 11, 1–6, 2015.
7. Liu, Q.-F., W.-Y. Yin, M.-F. Xue, J.-F. Mao, and Q.-H. Liu, "Shielding characterization of metallic enclosures with multiple slots and a thin-wire antenna loaded: multiple oblique EMP incidences with arbitrary polarizations," *IEEE Trans. Electromagn. Compat.*, Vol. 51, No. 2, 284–292, 2009.
8. Liu, Q.-F., W.-Y. Yin, J.-F. Mao, and Z.-Z. Chen, "Accurate characterization of shielding effectiveness of metallic enclosures with thin wires and thin slots," *IEEE Trans. Electromagn. Compat.*, Vol. 51, No. 2, 293–300, 2009.
9. Shi, Z. and P.-A. Du, "Numerical simulation of near field shielding properties for aperture arrays based on FEM," *Chin. J. Electron.*, Vol. 37, No. 3, 634–639, 2009.
10. Khorrami, M. A., P. Dehkhoda, R. M. Mazandaran, and S. H. H. Sadeghi, "Fast shielding effectiveness calculation of metallic enclosures with apertures using a multiresolution method of moments technique," *IEEE Trans. Electromagn. Compat.*, Vol. 52, No. 1, 230–235, 2010.
11. Dehkhoda, P., A. Tavakoli, and M. Azadifar, "Shielding effectiveness of an enclosure with finite wall thickness and perforated opposing walls at oblique incidence and arbitrary polarization by GMMoM," *IEEE Trans. Electromagn. Compat.*, Vol. 54, No. 4, 792–805, 2012.

12. Nie, B.-L., P.-A. Du, Y.-T. Yu, and Z. Shi, "Study of the shielding properties of enclosures with apertures at higher frequencies using the transmission-line modeling method," *IEEE Trans. Electromagn. Compat.*, Vol. 53, No. 1, 73–81, 2011.
13. Bethe, H. A., "Theory of diffraction by small apertures," *Physical Review Second Series*, Vol. 66, 163–182, 1944.
14. Rao, Y.-P., H. Song, and D.-F. Zhou, "Fast estimation of shielding efficiency of cavity with thin slots," *High Power Laser and Particle Beams*, Vol. 20, No. 8, 1327–1332, 2008.
15. Li, Y. Y. and C. Q. Jiao, "Analytical formulation for electromagnetic leakage from an apertured rectangular cavity," *PIERS Proceedings*, 257–261, Guangzhou, China, Aug. 25–28, 2014.
16. Liu, E.-B., P.-A. Du, and B.-L. Nie, "An extended analytical formulation for fast prediction of shielding effectiveness of an enclosure at different observation points with an off-axis aperture," *IEEE Trans. Electromagn. Compat.*, Vol. 56, No. 3, 589–598, 2014.
17. Luo, J.-W., P.-A. Du, D. Ren, and B.-L. Nie, "A BLT equation-based approach for calculating the shielding effectiveness of enclosures with apertures," *Acta Phys. Sin.*, Vol. 64, No. 1, 1–8, 2015.
18. Boutar, A., A. Reineix, C. Guiffaut, and G. Andrieu, "An efficient analytical method for electromagnetic field to transmission line coupling into a rectangular enclosure excited by an internal source," *IEEE Trans. Electromagn. Compat.*, Vol. 57, No. 3, 565–573, 2015.
19. Frederick, M. T., L. Michel, et al., *EMC Analysis Methods and Computational Models*, 1st edition, Wiley Interscience, New York, 1996.